Reconfigurable Circularly Polarized Antenna for Short-Range Communication Systems

Hakim Aïssat, Laurent Cirio, Marjorie Grzeskowiak, Jean-Marc Laheurte, and Odile Picon

***Abstract*—This paper describes the design rules of a compact microstrip patch antenna with polarization reconfigurable features (right-handed circular polarization (CP)/left-handed CP). The basic antenna is a circular coplanar-waveguide (CPW)-fed microstrip antenna excited by a diagonal slot and the CPW open end. This device is developed for short-range communications or contactless identification systems requiring polarization reconfigurability to optimize the link reliability. First, experimental and simulated results are presented for the passive version of the antenna excited by an asymmetric slot. A reconfigurable antenna using beam-lead p-i-n diodes to switch the polarization sense is then simulated with an electrical modeling of the diodes. Finally, the efficiency reduction resulting from the diode losses is discussed.**

***Index Terms*—Antenna diversity, circular polarization (CP), coplanar-waveguide (CPW) transitions, polarization switching.**

I. Introduction

A TREMENDOUS growth of the wireless RF identification (RFID) market is currently observed in the UHF and microwave bands. Dedicated frequency bandwidths in the UHF band are 865.6–867.6 MHz in the European Union, 902–928 MHz in the U.S., and 950–956 MHz in Japan. The microwave range is also considered at 5.8 GHz for electronic toll collection and more generally wireless road-to-vehicle communication systems. Simultaneously, there is a great interest in mobile *ad hoc* networks in which the routers are free to move randomly and organize themselves arbitrarily to form a self-configuring wireless network.

In short-range communications or contactless identification systems, antennas are key components, which must be small, low profile, and with minimal processing costs [1]. To cope with the unknown relative positions of the antennas in the *ad hoc* network or the RFID scenario, the antenna should also include some degree of radiation reconfigurability. More generally, diversity features can reduce the detrimental fading loss caused by multipath effects [2], [3]. This paper specifically focuses on polarization reconfigurability to optimize the link reliability.

In [2] and [3], a reconfigurable antenna was built from a dual-polarized aperture-coupled antenna, which used a 3-dB hybrid branch-line coupler as a polarizer to obtain circular polarization (CP). Boti *et al.* [4] proposed a compact single-feed switchable antenna with four beam-lead p-i-n diodes inserted directly on coupling slots, but with three metallization levels. To switch the polarization sense, Yang and Rahmat-Samii [5] used only two p-i-n diodes directly mounted on two orthogonal slots incorporated on the probe-fed patch antenna. In [6], the switching between right-handed circular polarization (RHCP) and left-handed circular polarization (LHCP) is obtained by turning ON/OFF two pairs of beam-lead p-i-n diodes soldered near an annular slot ring. With the same radiating structure, Ho *et al.* [7] used two p-i-n diodes on a uniplanar antenna where both the radiating element and feedline circuit were on the same layer.

We propose here an original and compact reconfigurable coplanar-waveguide (CPW) single-fed antenna, with only two metallization levels, dedicated to 5.8-GHz applications. No structure combining a CPW feeding and switching capabilities has been proposed yet for reconfigurable antennas. The CP sense is selected by four beam-lead p-i-n diodes directly inserted in the coupling cross slot below the radiating patch. By turning the pair of diodes ON or OFF, either RHCP or LHCP can be obtained with the same feeding line. Both passive and active structures are designed with a commercial code based on the finite-element method (Ansoft HFSS). To obtain accurate simulated results, the switching p-i-n diodes are modelled by an equivalent circuit where the electrical parameters (lumped resistor, inductor, and capacitor) are directly deduced from data provided by Agilent Technologies, Palo Alto, CA.

This paper is structured as follows. In Section II, the operation principle of the passive device is confirmed by CP measurements. In Section III, the reconfigurable device is numerically analyzed, taking into account the fine structure geometry and the accurate diode model. A set of relevant experiments are presented and discussed in relation to the structure details.

II. CP Passive Structure

In single-feed printed antennas, CP is generally obtained from two degenerate orthogonal linear polarizations with equal amplitude and 90° out-of-phase. For aperture-coupled patch antennas, the excitation can be provided by a coupling slot in the ground plane [8] or a modified cross slot and a bent tuning stub [9]. However, these structures need three metallization levels and increase the global height of the antenna. In [10], a tuning stub has been used on a compact circular radiating patch fed by a microstrip line. Chen *et al.* [11] have used circularly polarized printed shorted annular and square ring-slot antennas with a proximity coupling through a microstrip-line feed.

CPW feedings can also be used with similar performance with the attractive advantage of only two metallization layers and an easier integration of active devices. For instance, an asymmetrical CPW coupled slot with a slotted square patch is used in [12] and a CPW inset tuning stub in [13]. In all these antennas, an asymmetrical excitation mechanism is used to obtain CP.

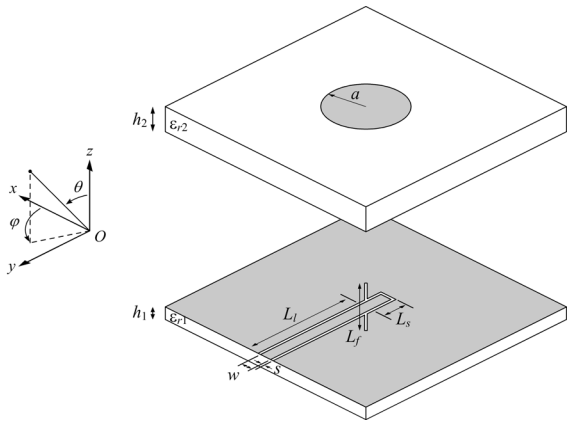

Fig. 1. CP antenna excited by a CPW feedline. $h_1 = 1.524$ mm, $\varepsilon_{r1} = 4.5$, $h_2 = 3.175$ mm, $\varepsilon_{r2} = 2.2$, $L_l = 30.4$ mm, $L_s = 5.3$ mm, $L_f = 17.6$ mm, $a = 9.2$ mm, $w = 1.8$ mm, $s = 0.3$ mm.

The CPW-fed structure proposed in this paper is also fed asymmetrically, but is much simpler (without a stub or slit on the radiating patch antenna) because of the use of a circular patch [14].

A. Antenna Design

In the circular-patch antenna proposed in Fig. 1 (where optimized dimensions have been determined after a parametric study described in Section II-D), CP can be achieved by combining two nonorthogonal linear polarized fields independently excited by an inclined slot and the open termination end of the CPW feed line [15].

Let us demonstrate this point by considering the field densities ($\vec{E}_1$) directed along Oy in the stub and ($\vec{E}_2$) oriented along $\varphi = +\pi/4$ in the diagonal slot. $\vec{E}_1$ and $\vec{E}_2$ expressions are given by

$$\vec{E}_1 = E_1 e^{j\phi} \vec{u}_y \tag{1}$$

$$\vec{E}_2 = E_2 \frac{\sqrt{2}}{2} \vec{u}_x + E_2 \frac{\sqrt{2}}{2} \vec{u}_y. \tag{2}$$

The total field is

$$\vec{E}_T = E_2 \frac{\sqrt{2}}{2} \vec{u}_x + \left(E_1 e^{j\phi} + E_2 \frac{\sqrt{2}}{2} \right) \vec{u}_y. \tag{3}$$

Applying the CP conditions $E_y = \pm j E_x$, one can easily deduce from (3) that CP is obtained for

$$\phi = \pi \pm \frac{\pi}{4} \text{ and } E_1 = E_2, \tag{4}$$

and the final field expressions are given by

$$(\text{RHCP})\vec{E} = E_1 \frac{\sqrt{2}}{2} \vec{u}_x + j E_1 \frac{\sqrt{2}}{2} \vec{u}_y \tag{5}$$

$$(\text{LHCP})\vec{E} = E_1 \frac{\sqrt{2}}{2} \vec{u}_x - j E_1 \frac{\sqrt{2}}{2} \vec{u}_y. \tag{6}$$

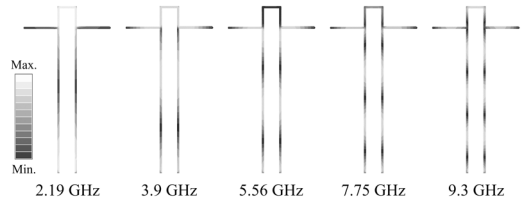

Fig. 2. Distribution of electric field for a CPW line with a perpendicular slot for various frequencies (no patch).

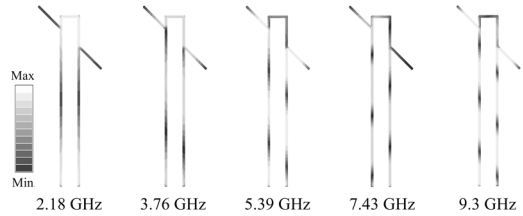

Fig. 3. Distribution of electric field for a CPW line with a 45° inclined slot for various frequencies.

We conclude that a 45° inclination of the coupling slot combined with a 180° ±45° phase difference and equal amplitude between the excited modes results in CP radiation (135° for RHCP, 225° for LHCP). Conversely, it can be easily shown that a −45° inclination of the coupling slot combined with a ±45° phase difference and equal amplitude between the excited modes also results in CP radiation (+45° for RHCP, −45° for LHCP).

Using the cavity model formulation [16], [17], a circular patch radius $a = 8.8$ mm is required for a 5.8-GHz resonant frequency using an RT/Duroid 5880 upper substrate ($\varepsilon_{r2} = 2.2$ and $h_2 = 3.175$ mm).

In the multilayer CPW design, closed-form expressions [18] and [19] resulting from a quasi-static analysis are used to determine frequency-independent values of the effective dielectric constant and characteristic impedance. The dimensions ($w = 1.8$ mm and $s = 0.3$ mm) are calculated to obtain a 50-Ω characteristic impedance with a TMM4 lower substrate ($\varepsilon_{r1} = 4.5$ and $h_1 = 1.524$ mm).

B. Feeding System and CP Characterization

The field distribution in the open-ended CPW line is first plotted for various frequencies with a perpendicular or a diagonal slot, but without a patch. Line dimensions are given in Fig. 1.

In Fig. 2, a perpendicular slot is used. Due to the slot symmetry with respect to the line, an identical field distribution is observed in both slot lines, i.e., only the odd mode can propagate. Depending on the frequency, the field is not necessarily maximum in the open stub when the dimensions of the perpendicular slot are resonant. At 5.56 GHz, the perpendicular slot essentially shorts the open stub and deviates the energy.

In Fig. 3, a 45° inclined slot loads the open-ended CPW line. The field distribution is no longer symmetrical in the line because of the excitation of the even mode and its combination with the odd mode. In this configuration, the field distribution and return loss depend on the line length between the symmetrical excitation and diagonal slot. As a matter of fact, this symmetrical excitation (for instance, coaxial probe) acts as a short

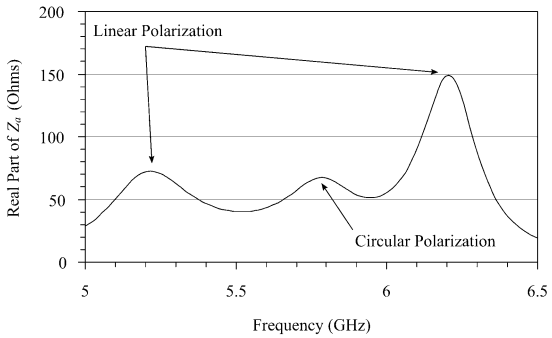

Fig. 4. Real part of the input impedance Za versus frequency (dimensions given in Fig. 1).

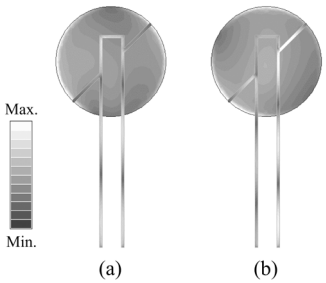

Fig. 5. Distribution of electric field in the CPW line and electric current on the patch (viewed from the backside).

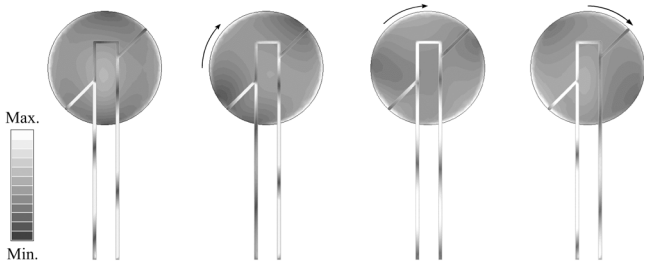

Fig. 6. Distribution of electric field in the CPW line and electric current on the patch at different time at 5.78 GHz (viewed from the backside).

circuit for the even mode. Therefore, the line length must also be taken into account in the antenna design. In addition, the frequency dependence of the field distribution in the open stub and the diagonal slot remains essentially the same as in Fig. 2.

We now consider the antenna of Fig. 1 including the circular patch and its feeding structure with a 45° inclined slot. The real part of the antenna input impedance Z_a is plotted on Fig. 4 in the 5–6.5-GHz band. Three peaks are observed at 5.22, 5.78, and 6.21 GHz.

The distributions of electric field in the feeding structure and electric current on the patch are plotted in Figs. 5 and 6.

At 5.22 GHz [see Fig. 5(a)], the electrical field is linearly polarized in the Oy-direction. The maximum energy is localized in the stub. The field does not see the diagonal slot. Therefore, the fields are symmetric in the feeding lines. At 6.21 GHz [see Fig. 5(b)], there is no energy in the stub. Due to the combination of odd and even modes propagating with different velocities, an asymmetrical field distribution is observed in the feeding line. The diagonal slot is excited and a linear polarization is obtained

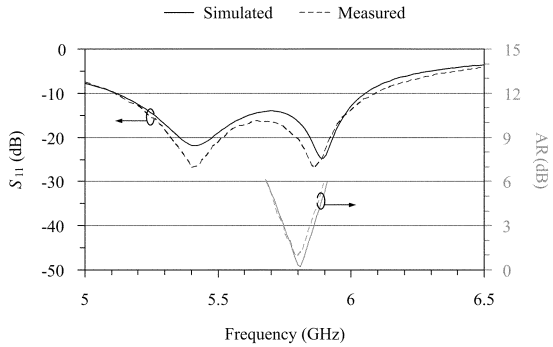

Fig. 7. Simulated and measured return loss and AR.

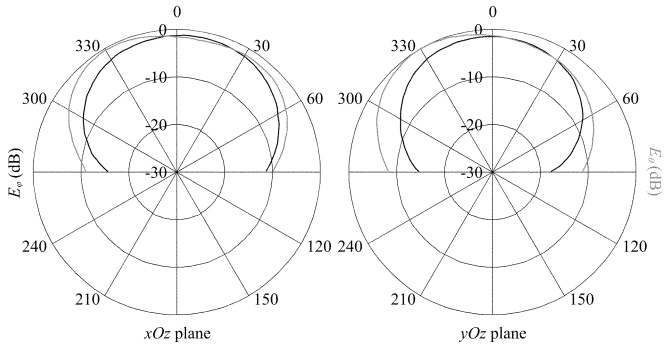

Fig. 8. Simulated radiation pattern at 5.8 GHz.

at 45°. At both frequencies, the linear polarization can be controlled by visualizing the time evolution of the electric current on the patch.

In Fig. 6, the current distribution is sequentially observed at different times at 5.78 GHz. A rotation of the current distribution is obtained with a maximum field located alternatively in the stub and slots. The polarization is RHCP, a $-45°$ inclined slot should be used for LHCP.

Making use of Fig. 4, it appears that the resonances at 5.22 and 6.21 GHz are associated with two degenerate linear polarizations, while the coupling between these yields a mode at an intermediate frequency (5.78 GHz) showing CP characteristics.

In Section II-D, it will be shown that the length of the stub is an important parameter to adjust the $180° \pm 45°$ phase difference and obtain CP.

C. Simulated and Measured Results

Fig. 7 describes the simulated and measured return loss (S_{11}) and axial ratio (AR) at boresight. The minimum AR occurs at the same frequency (5.8 GHz) for simulation and measurements. The measured AR is 1 dB, while the predicted AR was 0.3 dB. The measured AR and return-loss bandwidths are approximately 1.8% (AR $<$ 3 dB) and 18% ($S_{11} < -10$ dB), respectively.

The simulated and measured normalized radiation patterns for the minimum AR are, respectively, represented on Figs. 8 and 9. The measured passive antenna gain is 6.9 dB.

A good agreement is observed between simulated and measured results for the passive structure with similar E_θ and E_φ levels around boresight.

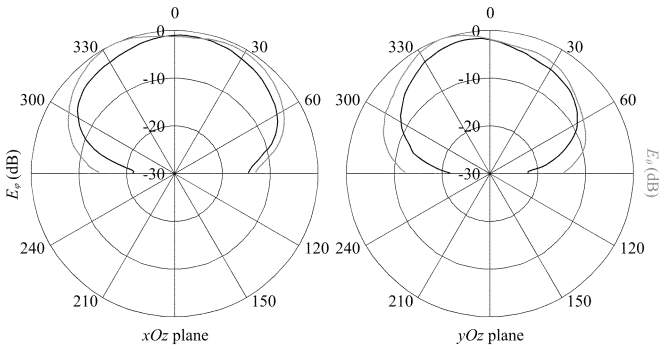

Fig. 9. Measured radiation pattern at 5.8 GHz.

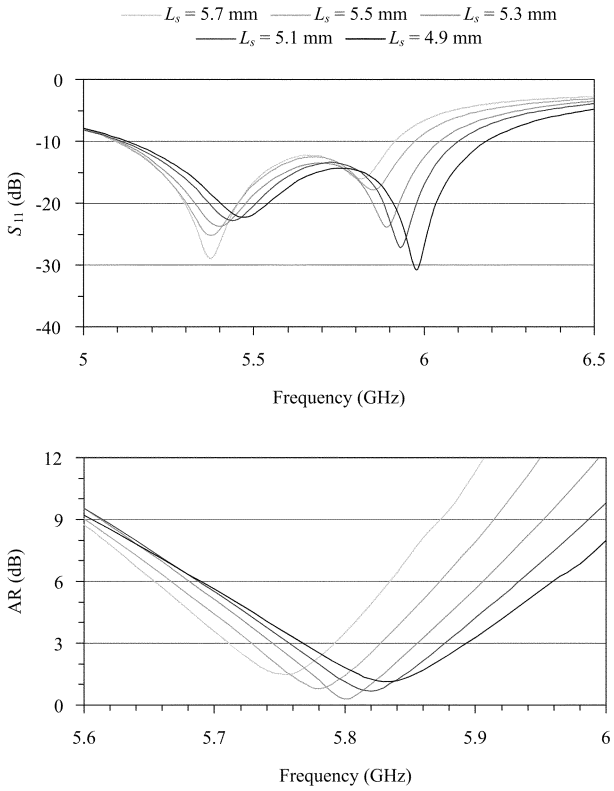

Fig. 10. Effect of the CPW open stub length.

The dimensions of the final prototype given in Fig. 1 have been optimized with the parametric study (essentially the length of the coplanar line and open stub) described in Section II-D.

D. Parametric Study

We first consider the effect of the CPW open stub length (L_s) on the antenna performance (Fig. 1). The CPW length (L_l) and slot length (L_f) are, respectively, set to a constant of 30.4 and 17.6 mm. L_s is chosen to have five different values, i.e., 4.9, 5.1, 5.3, 5.5, and 5.7 mm. The effects of L_s on S_{11} and AR are shown on Fig. 10. These curves indicate that the stub length controls the phase difference ϕ between the linear polarizations. A minimum AR (0.28 dB) appears at 5.8 GHz for $L_s = 5.3$ mm and it rapidly degrades around this value (1.2 and 1.54 dB, respectively, for $L_s = 4.9$ and 5.7 mm).

The axial ratio bandwidth (ARBW) increases as L_s decreases (1.89% and 2.15%, respectively, for $L_s = 5.3$ and 4.9 mm)

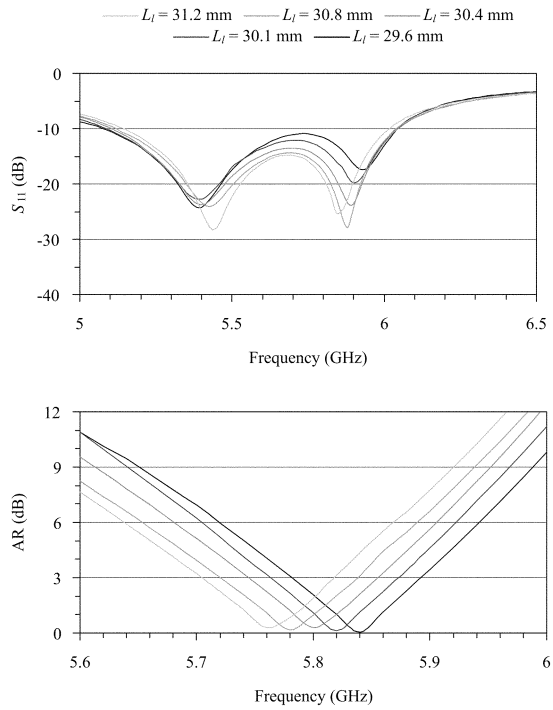

Fig. 11. Effect of the CPW feedline length.

allowing an optimization of the ARBW to the detriment of the minimum AR level.

The return loss shows two specific minimum corresponding to the linear polarizations above and below the CP frequency of interest. Both resonant frequencies are shifted as L_s varies and affect the impedance matching at the frequency corresponding to the minimum AR. However, the antenna remains always matched for the L_s values chosen here ($S_{11} < -10$ dB).

The variation of S_{11} and AR levels versus CPW feedline length (L_l) is depicted in Fig. 11 for five values (L_s and L_f are, respectively, set to 5.3 and 17.6 mm). As L_l decreases (from 31.2 to 29.6 mm), the frequency corresponding to the minimum AR increases (from 5.76 to 5.84 GHz) maintaining a good CP purity ($\mathrm{AR} < 0.3$ dB) and a constant ARBW (1.9%). This is due to the constant shift of the linear polarization resonant frequencies around the minimum AR, which are moved to higher frequencies as L_l decreases.

The return loss remains below -10 dB at the minimum AR frequency while both minimum locations are not significantly altered by L_l.

Other parametric studies on the slot length L_f and the radius a have also been used in the antenna design.

III. Antenna With Switchable Polarization Sense

A. Topology of the Reconfigurable Antenna

The antenna with polarization diversity is derived from the passive structure by adding a symmetrical slot along the second diagonal [20], as represented in Fig. 12.

Slots, stubs, and patch dimensions are kept identical. Each slot can be short circuited by means of a pair of beam-lead p-i-n diodes (HPND-4028 Agilent Technologies, Palo Alto, CA) located near the intersection with the feeding line and directly

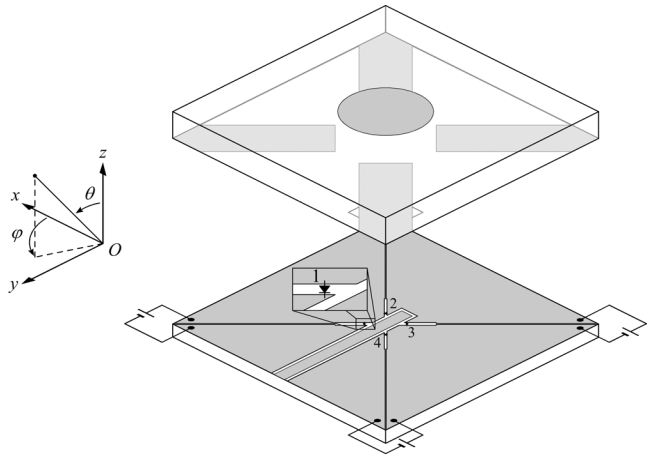

Fig. 12. Circularly polarized reconfigurable structure.

soldered in the coupling slots. By switching on a pair of diodes while the other is OFF, the antenna can switch between the RHCP and LHCP states with a single feeding port. In Fig. 12, shorting diodes 1 and 3 (2 and 4, respectively) produces RHCP (LHCP, respectively).

The dc-bias voltage is supplied through a divided ground plane, separated into five parts using four thin slits (130 μm). As a biasing circuit must not affect the RF behavior of the antenna, large capacitors are built over the slits by stacking copper strips and adhesive tapes (upper layer on Fig. 12). The slits are first covered by an isolating adhesive layer (approximately 130-μm thickness), which insures a dc isolation maintaining RF continuity. The adhesive layer is then topped with four copper tapes to shield the slits at RF frequencies.

The effect of the second slot and the influence of the diode positions are studied in Section III-B. A second study is performed in Section III-C to assess the capacity value due to the thin air gap layer. In Section III-D, simulations of the reconfigurable antenna are performed with ideal models of the diodes. Comparisons with the measured switchable prototype are presented and the validity of the ideal model is discussed. In Section III-E, an equivalent circuit of the diode is implemented in the High Frequency Structure Simulator (HFSS) software with electrical parameters directly deduced from data provided by Agilent Technologies. Finally, in Section III-F, the efficiency reduction resulting from the integration of the diodes is discussed.

B. Effect of the Diode Position

Here, the switch position inside the coupling slots is modified to control its effect on S_{11} and AR. This study is useful to estimate the tolerance of the switchable antenna toward inaccurate soldering and placement of the diodes.

To perform the parametric study, an ideal model of the diode is implemented. As 110 μm is the average width of the beam-lead p-i-n diode, a 110-μm-wide metallic strip is used to model the p-i-n diode in the forward state (Fig. 13). An infinite resistance models the diode in the reverse state. In Fig. 14, the simulated S_{11} and AR are reported for the antenna with a single inclined slot (passive antenna described in Section II). A second simulation is performed with two perpendicular slots and a short

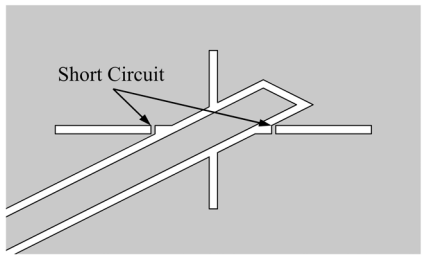

Fig. 13. Position of the ideal short circuit in the slots.

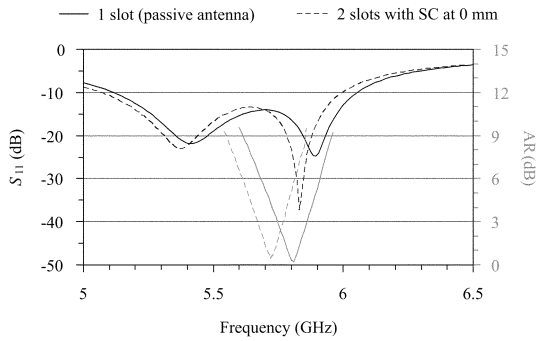

Fig. 14. Influence of the second slot including ideal short circuits.

TABLE I
AR VERSUS SWITCH POSITION

	Frequency	AR
Antenna with 1 slot (passive antenna)	5.81 GHz	0.20 dB
2 slots antenna with SC at 0 mm	5.72 GHz	0.43 dB
2 slots antenna with SC at 0.5 mm	5.74 GHz	0.26 dB
2 slots antenna with SC at 1 mm	5.74 GHz	0.30 dB
2 slots antenna with SC at 1.5 mm	5.74 GHz	0.84 dB
2 slots antenna with SC at 2 mm	5.74 GHz	1.84 dB

circuit located at a distance $d = 0$ mm from the CPW feeding line (Fig. 13).

A 1.5% frequency shift of the minimum AR (5.72 GHz instead of 5.81 GHz for the single slot) and similar matching levels (-15 and -17 dB, respectively) are observed in Fig. 14. The AR level is not significantly altered by the presence of the second slot and the switch (0.43 dB instead of 0.2 dB).

In Table I, the minimum AR level and the associated frequency are given for different diode positions. From $d = 0$ mm to 1 mm, the AR level is correct (below 0.5 dB), but degrades with larger distances reaching only 1.84 dB for $d = 2$ mm. We conclude that the switching diodes must be soldered as close as possible to the CPW feedline with a maximum tolerance $d = 1$ mm.

C. Air-Gap Influence

Due to the isolating adhesive layer, a 130-μm-thick air gap is introduced between the ground plane and the RT/Duroid 5880 substrate. To evaluate the influence of this third dielectric layer, simulated results obtained with two antenna configurations have been plotted in Fig. 15. One is the antenna simulated in Fig. 14 (dotted line) with two perpendicular slots and an ideal short circuit. The other antenna is identical to the previous one, but includes the dc-bias circuit (divided ground plane with four thin slits, 130-μm air gap layer and four copper tapes).

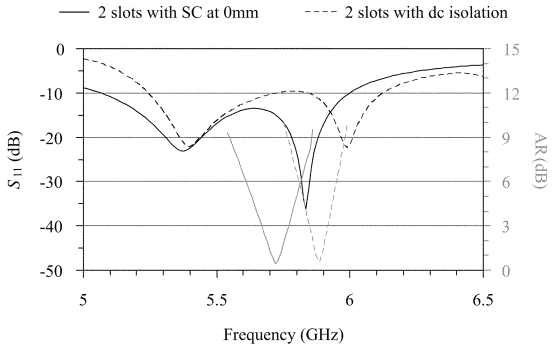

Fig. 15. Influence of the dc isolation circuit.

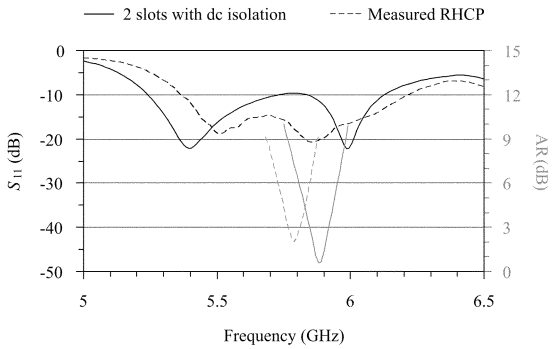

Fig. 16. Measured and simulated S_{11} and AR results with an ideal diode modeling.

In Fig. 15, the CP purity is nearly identical for both simulations (minimum $\mathrm{AR} = 0.42$ and 0.57 dB with dc isolation circuit) with moderate S_{11} level differences (-14 and -11.3 dB with dc isolation). However, an important frequency shift of the minimum AR is observed (from 5.72 to 5.88 GHz). The same decay is observed on S_{11} on the second minimum location. We conclude that the relative thinness of the air gap layer (130 μm) compared to the RT/Duroid 5880 thickness (3.175 mm) cannot be neglected and must be modeled as a third layer inserted between both dielectric layers.

D. Simulation Based on Ideal Diodes—Comparison With Measurements

The reconfigurable antenna including two pairs of diodes has been designed and fabricated. Experimental results are reported in Fig. 16 and compared with simulated results including the biasing circuit and obtained with ideal diodes. In the HFSS software, the diodes in the ON state are modeled by a 110-μm-wide metallic strip and the diodes in the OFF state are modeled by an open circuit. In the simulation and measurements, diodes 1 and 3 are in the ON state, while diodes 2 and 4 are in the OFF state (RHCP pattern).

The minima AR are 0.57 dB at 5.88 GHz (simulation) and 2 dB at 5.79 GHz (measurement), respectively. The corresponding return losses are -11.3 dB (simulation) and -17.9 dB (measurement), respectively. The frequency shift and level degradation of AR minima result in a 1.43-dB difference of the minimum AR level and a 1.5% frequency shift. As the antenna under consideration is characterized by a narrow 1% ARBW for an AR < 3-dB criterion, the prediction does not comply to design purposes.

TABLE II
TYPICAL S-PARAMETERS AT 6 GHz (AGILENT TECHNOLOGIES DATA)

6 GHz	S_{11}/S_{22}		S_{12}/S_{21}	
	Mag.	Ang.	Mag.	Ang.
I_F = 1 mA	0.069	46	0.956	-7
I_F = 5 mA	0.064	57	0.971	-7
I_F = 10 mA	0.063	60	0.974	-7
V_R = 0 V	0.921	-21	0.219	60
V_R = 10 V	0.979	-16	0.131	75
V_R = 30 V	0.982	-15	0.12	76

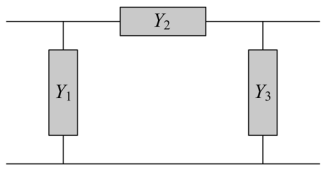

Fig. 17. π electrical network.

The discrepancy between experimental and simulated results is attributed to the parasitic reactance and losses of the diode, which are not included in the simulation. The improvement of the diode modeling is covered in Section III-E.

E. Simulation Using Equivalent Circuits of the Diode

Here, an electrical model of the HPND-4028 beam-lead diode is integrated into the HFSS simulator. One simulator constraint is that only parallel circuits (resistor R_P, inductor L_P, and capacitor C_P) can be included. For both forward and reverse states, the values of the lumped elements (R_P, L_P, and C_P) have been extracted from the S-parameters provided by Agilent Technologies at 6 GHz and given in Table II for different dc-bias values.

The beam-lead p-i-n diodes require a forward bias current I_F in the forward state (ON) and a reverse voltage V_R in the reverse state (OFF). Using Table II, the biasing current $I_F = 10$ mA and reverse voltage $V_R = 10$ V have been selected.

The S-parameters have been measured in a series configuration with microstrip ports [21]. The equivalent electrical circuit (π electrical network) depicted in Fig. 17 is particularly suitable here. The open-end effects are modeled by $Y_1 = Y_3$, while the diode behavior is included in Y_2. Using $[S]$-to-$[Y]$ conversion tables for the two-port network, Y_1 and Y_2 are identified at 6 GHz.

As the diode environment is different in the Agilent Technologies' setup (microstrip ports) and the reconfigurable antenna (soldered in a slot), only Y_2 was taken into account to determine the equivalent parallel circuit (R_P, L_P, and C_P).

In Table III, the real and imaginary parts of Y_2 are given with the lumped elements R_P, L_P, C_P of the equivalent parallel circuit.

A simple capacitor C_P is needed in the OFF state, while two lumped elements (R_P and L_P) are required to model the switch in the ON state. In Fig. 18, simulated and measured S_{11} and AR are plotted versus frequency with the RHCP configuration.

An excellent agreement with measurements is observed in AR simulations. The simulated minimum $\mathrm{AR} = 1.11$ dB is obtained at 5.78 GHz with $S_{11} = -11.3$ dB and $\mathrm{ARBW} = 0.82\%$. Measurements indicate a minimum $\mathrm{AR} = 2$ dB obtained at 5.79 GHz with $S_{11} = -17.8$ dB and $\mathrm{ARBW} = 0.8\%$.

TABLE III
LUMPED ELEMENTS OF THE EQUIVALENT PARALLEL CIRCUIT AT 6 GHz

Forward State	Reverse State
Y_2 = 0.028 - 0.102j	Y_2 = 0 + 0.001358j
R_P = 35.7 Ω L_P = 260.1 pH	C_P = 36.02 fF

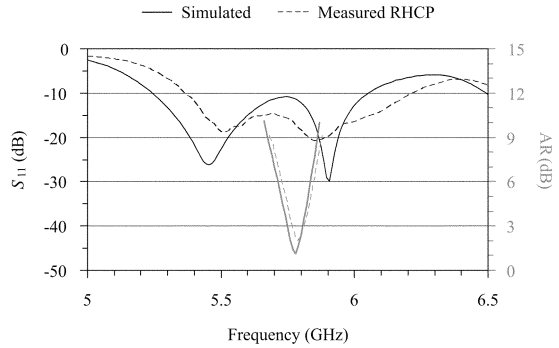

Fig. 18. Results of S_{11} and AR with an electrical model of the diode.

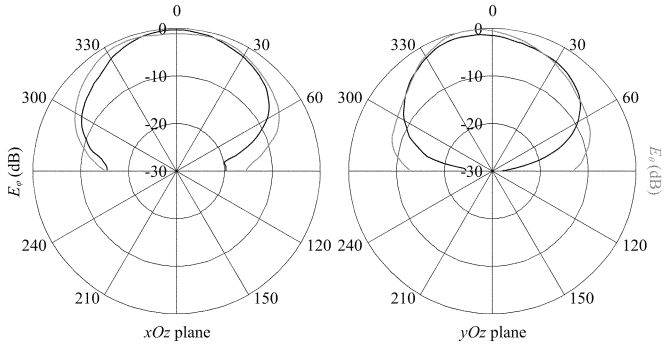

Fig. 19. Measured radiation pattern at 5.79 GHz.

A comparison can be made with results of Fig. 15 obtained with an ideal model of the diode. A sensible improvement is clearly obtained with an electrical model of the switch. The difference between the simulation and measurements drops from 1.43 to 0.89 dB for the AR level and from 1.5% to 0.2% for the frequency shift.

The measured far-field patterns obtained at 5.79 GHz is displayed in Fig. 19 for the RHCP state. As revealed by the graph, the radiation patterns are very close to the patterns of the passive patch antenna (Fig. 9). Similar curves (not shown here) were obtained for LHCP.

These results clearly show a significant improvement of the simulated results when an electrical model of the diode is used. On the other hand, the parasitic radiation of the diode is not taken into account in the electrical model, which probably causes an AR degradation. Moreover, some limitations of the switch components must be taken into account. For example, the losses and power limitations of the diodes inserted in the reconfigurable antenna require some consideration.

F. Diode Effects on the Radiation Efficiency

The measured gain of the reconfigurable antenna is 6.02 dB. This decrease, comparative to the 6.9 dB of the passive antenna, is significant and cannot be related to the lower reflection coefficient (−17.8 dB versus −20.4 dB). Assuming identical directivities for the passive and active reconfigurable antennas, the $6.9 - 6.02 = 0.88$ dB difference corresponds to a drop of antenna efficiency. Even though the efficiency of the passive antenna has not been measured (typically around 90%), the previous comparison indicates that the efficiency decrease $(1 - 10^{-0.88/10} = 18\%)$ results from the diodes integration. This decrease is not only attributed to the losses in the diode, but also to the excitation of CP cross-polarization observed through the AR degradation in the reconfigurable antenna.

TABLE IV
AR AND GAIN OF THE RECONFIGURABLE ANTENNA VERSUS INPUT POWER

Power (dBm)	AR (dB)	Gain (dB)
16	2.06	6.02
18	2.05	6.02
20	2.06	6.01
22	2.09	5.99
24	2.17	5.94
26	2.55	5.82

Extra measurements have been done to emphasize the influence of the nonlinearity of the diodes for several power levels in a transmitter configuration. In these measurements, the reconfigurable antenna is used as a transmitter antenna and fed by a power generator, of which output power level ranges from 16 to 26 dBm. Results are given in Table IV.

No significant variations of the gain and AR values are observed for power levels lower than 22 dBm. For higher power levels, both gain and AR performances degrade. This degradation is attributed to the nonlinearities of the diodes, which alters the phase and amplitude conditions to obtain the CP operation of the antenna.

IV. CONCLUSION

A reconfigurable CPW-single fed antenna has been developed for short-range communication systems requiring CP diversity or modulation. To obtain a compact structure, switchable devices (four p-i-n diodes) have been directly integrated below the radiating element on the CPW feeding line. The resulting reconfigurable antenna is compact with a biasing circuit and components located inside the radiating parts of the structure. After a detailed study of the passive structure, we have demonstrated that a great improvement of the AR prediction is obtained with an equivalent circuit of the diode. For antennas showing narrow ARBW, simple shorts or opens are not sufficient for the diode modeling. The switchable polarization sense has been clearly demonstrated in a 5.8-GHz prototype and its potential integration in RFID systems has been highlighted.

ACKNOWLEDGMENT

The authors would like to thank D. Delcroix, Equipe Systèmes de Communication et Microsystèmes (ESYCOM) Laboratory, Marne-la-Vallée, France, and D. Vandermoere, Institut d'Electronique de Microélectronique et de Nanotechnologie (IEMN), Lille, France, for the antennas realizations.

REFERENCES

[1] M. Hirvonen, P. Pursula, K. Jaakkola, and K. Laukkanen, "Planar inverted-F antenna for radio frequency identification," *Electron. Lett.*, vol. 40, no. 14, pp. 848–850, Jul. 2004.

[2] M. Kossel, H. Benedickter, W. Bächtold, R. Küng, and J. Hansen, "Circularly polarized, aperture-coupled patch antennas for a 2.4 GHz RF-ID system," *Microw. J.*, vol. 42, no. 11, pp. 20–44, Nov. 1999.

[3] M. Kossel, R. Küng, H. Benedickter, and W. Bächtold, "An active tagging system using circular-polarization modulation," *IEEE Trans. Microw. Theory Tech.*, vol. 47, no. 12, pp. 2242–2248, Dec. 1999.

[4] M. Boti, L. Dussopt, and J.-M. Laheurte, "Circularly polarised antenna with switchable polarisation sense," *Electron. Lett.*, vol. 36, no. 18, pp. 1518–1519, Aug. 2000.

[5] F. Yang and Y. Rahmat-Samii, "A reconfigurable patch antenna using switchable slots for circular polarization diversity," *IEEE Microw. Wireless Compon. Lett.*, vol. 12, no. 3, pp. 96–98, Mar. 2002.

[6] M. K. Fries, M. Gräni, and R. Vahldieck, "A reconfigurable slot antenna with switchable polarization," *IEEE Microw. Compon. Lett.*, vol. 13, no. 11, pp. 490–492, Nov. 2003.

[7] M.-H. Ho, M.-T. Wu, and C.-I. G. Hsu, "An RHCP/LHCP switchable slotline-fed slot-ring antenna," *Microw. Opt. Technol. Lett.*, vol. 46, no. 1, pp. 30–33, Jul. 2005.

[8] C.-Y. Huang, J.-Y. Wu, and K.-L. Wong, "Slot-coupled microstrip antenna for broadband circular polarisation," *Electron. Lett.*, vol. 34, no. 9, pp. 835–836, Apr. 1998.

[9] K.-L. Wong and M.-H. Chen, "Small slot-coupled circularly-polarised microstrip antenna with modified cross-slot and bent tuning stub," *Electron. Lett.*, vol. 34, no. 16, pp. 1542–1543, Aug. 1998.

[10] K.-L. Wong and Y.-F. Lin, "Circularly polarised microstrip antenna with a tuning stub," *Electron. Lett.*, vol. 34, no. 9, pp. 831–832, Apr. 1998.

[11] W.-S. Chen, C.-C. Huang, and K.-L. Wong, "Microstrip-line-fed printed shorted ring-slot antennas for circular polarization," *Microw. Opt. Technol. Lett.*, vol. 31, no. 2, pp. 137–140, Oct. 2001.

[12] C.-Y. Huang and K.-L. Wong, "Coplanar waveguide-fed circularly polarized microstrip antenna," *IEEE Trans. Antennas Propag.*, vol. 48, no. 2, pp. 328–329, Feb. 2000.

[13] C.-Y. Huang, "A circularly polarized microstrip antenna using a coplanar-waveguide feed with an inset tuning stub," *Microw. Opt. Technol. Lett.*, vol. 28, no. 5, pp. 311–312, Mar. 2001.

[14] H. Aïssat, L. Cirio, M. Grzeskowiak, and O. Picon, "Circularly polarized microstrip antenna coupled on an asymmetrical cross coplanar slot," in *Proc. 20th Int. Antennas Symp.*, Nice, France, Nov. 12–14, 2002, pp. 137–140.

[15] H. Aïssat, L. Cirio, M. Grzeskowiak, J.-M. Laheurte, and O. Picon, "Circularly polarized antenna excited by coplanar waveguide feedline," *Electron. Lett.*, vol. 40, no. 7, pp. 402–403, Apr. 2004.

[16] L. C. Shen, S. A. Long, M. Allerding, and M. Walton, "Resonant frequency of a circular disc, printed-circuit antenna," *IEEE Trans. Antennas Propag.*, vol. 25, no. 4, pp. 595–596, Jul. 1977.

[17] C. A. Balanis*, Advanced Engineering Electromagnetic*. New York: Wiley, 1989, pp. 492–499.

[18] W. Hilberg, "From approximation to exact relations for characteristic impedances," *IEEE Trans. Microw. Theory Tech.*, vol. 17, no. 5, pp. 259–265, May 1969.

[19] S. S. Bedair and I. Wolff, "Fast, accurate and simple approximate formulas for calculating the parameters of supported coplanar waveguides for (M)MICs," *IEEE Trans. Microw. Theory Tech.*, vol. 40, no. 1, pp. 41–48, Jan. 1992.

[20] H. Aïssat, L. Cirio, M. Grzeskowiak, J.-M. Laheurte, and O. Picon, "CPW-fed patch antenna with switchable polarization sense," in *Proc. 35th Eur. Microw. Conf.*, Paris, France, Oct. 4–6, 2005, CD ROM, Abstract p. 104.

[21] "Beam lead PIN diodes for phased arrays and switches," Agilent Technol., Palo Alto, CA, HPND-4028, HPND-4038, Data sheet, 1999 [Online]. Available: http://www.agilent.com

Hakim Aïssat was born in Le Blanc-Mesnil, France, in 1976. He received the M.Sc. degree in electrical engineering from the Université de Marne-la-Vallée, Marne-la-Vallée, France, in 2000, and is currently working toward the Ph.D. degree in electrical engineering at the Université de Marne-la-Vallée.

His research interests include electromagnetic numerical modeling and antenna design and measurement.

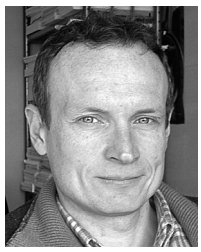

Laurent Cirio was born in Nogent-sur-Marne, France, on May 1966. He received the Ph.D. degree in electrical engineering from the Laboratoire d'Electronique, Antennes et Télécommunications (LEAT), University of Nice-Sophia Antipolis, Nice-Sophia Antipolis, France, in 1994. His doctoral thesis concerned the modeling of microstrip antenna with polarization switching capability using the transmission line matrix (TLM) method and parallel computer.

In 1996, he joined the Equipe Systèmes de Communication et Microsystèmes (ESYCOM) Laboratory, University of Marne-la-Vallée, Marne-la-Vallée, France, as an Assistant Professor. His research focuses on planar antennas with diversity capabilities, printed lines on silicon substrates, and temporal numerical methods applied on microwave structures. He is also involved with experimental characterization and antenna measurement.

Marjorie Grzeskowiak was born in Douai, France, in 1973. She received the Ph.D. degree in electrical engineering from the University of Science and Technology of Lille (USTL), Lille, France, in 1999.

Since 2000, she has been an Assistant Professor with the Equipe Systèmes de Communication et Microsystèmes (ESYCOM) Laboratory, University of Marne-la-Vallée, Marne-la-Vallée, France. Her subjects of interest concern the conception of RF and millimeter antennas for RF identification (RFID) applications, ultra-wideband (UWB) systems, and electromagnetic energy conversion with active components [diodes or micro-electromechanical systems (MEMs)].

Jean-Marc Laheurte received the M.Sc. and Ph.D. degrees in electrical engineering and Habilitation à Diriger les Recherches degree from the University of Nice, Nice, France, in 1989 and 1992, and 1997, respectively.

In 1989 and 1990, he was a Research Assistant with the Ecole Polytechnique Fédérale of Lausanne, Lausanne, Switzerland. From 1992 to 1993, he was a Post-Doctoral Researcher with The University of Michigan at Ann Arbor. From 1993 to 2002, he was an Assistant Professor with the University of Nice. In 2002, he joined the Equipe Systèmes de Communication et Microsystèmes (ESYCOM) Laboratory, University of Marne-la-Vallée, Marne-la-Vallée, France, where he is currently a Professor of electrical engineering in charge of the development of antenna activities. In 2005, he was a Visiting Professor with the Laboratoire de Physique de la Matière Condensée (UNSA). He has authored or coauthored over 40 technical papers and 50 conference papers. His research interests include numerical modeling of microstrip structures, design of active antennas, antenna diversity, and electromagnetic-bandgap (EBG)- and microelectromechanical systems (MEMS)-based antenna concepts.

Dr. Laheurte was the recipient of the 1991 Jeunes et Antennes Award from the Société des Electriciens et Electroniciens (SEE). He was also the recipient of a 1993 Lavoisier Fellowship.

Odile Picon (M'86) was born in Paris, France. She received the Agregation de Physique degree from the Ecole Normale Supérieur, Fontenay aux Roses, France, in 1976, the Doctor degree in external geophysics from the University of Orsay, Orsay, France, in 1980, and the Doctor in physics degree from the University of Rennes, Rennes, France, in 1988.

From 1976 to 1982, she was a Teacher. From 1982 to 1991, she was a Research Engineer with the Space and Radioelectric Transmission Division, Centre National d'études des télécommunications. From 1991 to 1993, she was a Professor of electrical engineering with Paris7 University. Since 1994, she has been a Professor or electrical engineering with the University of Marne-la-Vallée, Marne-la-Vallée, France, where she heads the Equipe Systèmes de Communication et Microsystèmes (ESYCOM) Laboratory. Her research deals with electromagnetic theory and numerical methods for solving field problems and design of millimeter wave passive devices.